Design of Control Strategies for a Low Voltage DC Residential Grids

Guilherme M. Paraíso, MSc Student, IST; J. Fernando A. Silva, Senior Member, IEEE, and Sónia F. Pinto, Senior Member, IEEE

***Abstract*— In recent years there has been an increasing interest in DC distribution networks to replace or complement the traditional AC distribution networks.**

The purpose of this thesis is to design a DC distribution grid consisting of a DC power source and a Buck converter. This converter must be able to control and regulate the voltage on the DC bus after the connection of Constant Power Loads (CPLs). In order to do so, 2 non-linear control systems were designed.

The first proposed controller is a combination of two non-linear control techniques based on the Lyapunov Stability Theory and is called Backstepping Sliding Mode Controller (BSMC). The second control system uses only the non-linear Backstepping control technique and is called Recursive Backstepping Controller (RBC).

These 2 control strategies are then compared in terms of overvoltages / undervoltages and transient responses. Simulations and results obtained experimentally confirm the best performance is obtained with BSMC which is based on nonlinear control theory.

***Index Terms*—DC Microgrid, Buck Converter, Linear Controllers, Non-Linear Controllers, Backstepping Control, Sliding Mode Control**

I. Introduction

In recent years with the advancement in semiconductor technology that allowed to step-up or step-down DC voltage, DC networks are a possible solution to replace or complement the traditional AC distribution system [1]. These DC grids may become an important asset to integrate Renewable Energy (RE) such as photovoltaic, which intrinsically produce DC. With the penetration of these RE sources arises the need for distributed power systems to be equipped with Energy Storage Systems (ESSs) capable of compensating the differences between generated and consumed power. Therefore, DC microgrids have an advantage because it is easier to integrate these ESSs, as most of them require the connection to DC [2].

Most of the household appliances as: laptops, TV's, tablets, phones and newer lighting systems use DC power [3]. Supplying these loads through the conventional AC distribution network requires additional DC-AC conversion stages [4], with the consequent power losses. However, with a DC system the number of conversion stages would be reduced which will, therefore, decrease the cost of implementation and leading to a higher efficiency.

One of the main challenges for DC distribution grids is to deal with the interaction between power electronic loads mainly constant power loads. They will have a great impact on the stability and robustness of the DC microgrid due to its negative impedance characteristic [5] [6] [7].

Several methods have been proposed to control microgrids and to counteract instabilities caused by CPLs. Among them are, passivity-based control, which uses passive elements to dampen the oscillations of the system, active damping [8], a solution that involves a modification in the control loop by creating a damping effect of passive damping or modifying the DC bus capacitance. Many nonlinear control methods have also been applied to overcome this problem such as, feedback linearization [9], where a nonlinear model of the system is linearized by defining appropriate state-variables, sliding mode controllers [10] operating at a variable frequency to guarantee that the variables to control can track a certain reference path.

II. Modeling the DC Distribution Grid

The DC distribution grid is considered to be fed from a DC power source (e.g. a renewable energy system with storage). The DC power supply then supplies the grid main DC-DC buck converter (Fig. 1). This power converter will be used to control the DC grid voltage V_o and limit the short-circuit current by acting on the switching transistor duty-cycle.

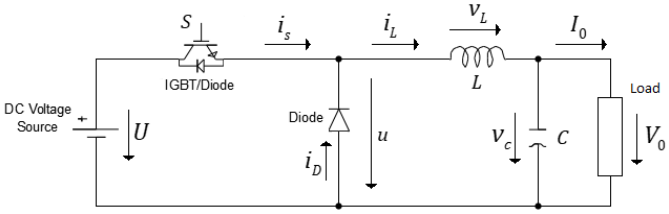

Fig. 1 – Main DC-DC Buck converter

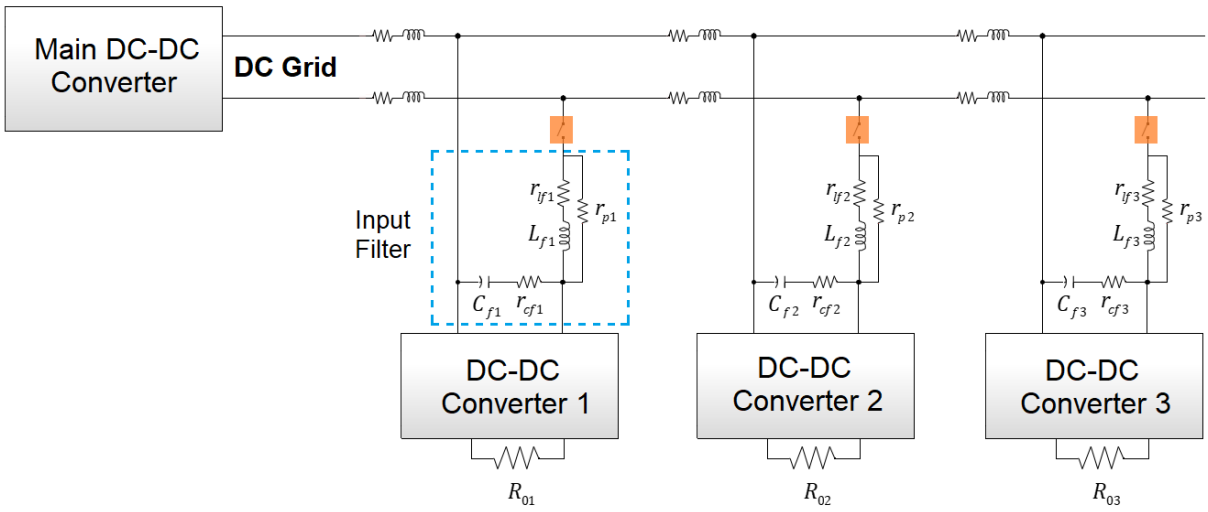

Fig. 2 – DC Grid Representation

The characteristic loads of this grid will be other power converters feeding loads, such as computers, screens set, phones, that can be considered to absorb a constant power at a given operating point, due to the relatively small switching periods of the power converters. Therefore, the load converters operate at constant power, and in steady-state, at constant number of loads the main converter will be operated at constant power ($dP_0 = 0$), which means that:

$$P_0 = V_0 I_0 = constant \tag{1}$$

This behavior may be regarded as a negative incremental resistance r_i [11],, that can be defined as:

$$dP_0 = V_0 dI_0 + I_0 dV_0 = 0 \Leftrightarrow \frac{V_0}{I_0} = -\frac{dV_0}{dI_0} = r_i \tag{2}$$

Therefore, if the voltage across the capacitor increases/decreases, the current that flows through the load will decrease/increase respectively. This can be the cause of instability in the DC grid voltage.

Different loads will be connected to the DC bus through different lines with negligible losses. Each load is often a Buck converter with its own output power and input filter. These input filters are necessary to avoid the converter switching current pulses from being reflected back into the line, attenuating the switching harmonics from the line present in the converter input current [12]. The DC grid and load representation can be seen in Fig. 2.

III. Non-Linear Controllers

In this chapter, two non-linear design controllers are presented to control the DC grid main DC-DC converter based on Lyapunov's second method [13] for stability at constant power loads.

1) *Backstepping Sliding Mode Control*

This control approach combines Backstepping and Sliding Mode Control (BSMC) [13] [14] [15]: the voltage controller (outer loop), that will define the inductor's current i_{Lref} needed to follow a reference voltage (V_0=V_{0ref}) using Backstepping theory; and the current controller (inner loop), which is based in Sliding Mode Control to force the current tracking behavior ($i_L = i_{Lref}$).

a) *Backstepping Voltage Controller*

The average model of the buck converter represented in Fig. 1 can be written as:

$$\begin{cases} \dot{v}_C = \dfrac{i_L - I_0}{C} \\ \dot{i}_L = \dfrac{u - v_C}{L} \end{cases} \tag{3}$$

Our control goal is to force the output v_c, to track a reference signal v_{cref}. The tracking error associated to this objective and its derivative can be defined as:

$$e_{v_C} = v_{c_{ref}} - v_c \tag{4}$$

$$\frac{de_{v_C}}{dt} = \frac{dv_{Cref}}{dt} - \frac{i_L - I_0}{C} \tag{5}$$

Consider the following candidate Lyapunov function:

$$V_L = \frac{e_{v_C}^2}{2} \tag{6}$$

A standard quadratic function, positive definite and radially unbounded. By application of Lyapunov's Second Method the system is asymptotically stable if:

$$\dot{V}_L = e_{v_C} \frac{de_{v_C}}{dt} = -k_v e_{v_C}^2 \tag{7}$$

where k_v is a positive constant. Then i_L is regarded as the virtual control input in (5) and its desired value denoted as i_{Lref}. After some manipulations i_{Lref} is obtained:

$$i_{Lref} = Ck_v e_{v_C} + C\frac{dv_{Cref}}{dt} + I_0 \tag{8}$$

To guarantee zero static error that may occur due to parameter mismatch or measuring errors in (8), one possible solution, is to extend the previous procedure and add the integral of the error e_{vC} in the Lyapunov function and ensuring that is 0. By defining a new Lyapunov function:

$$V_{L1} = k_I \frac{e_I^2}{2} + \frac{e_{vC}^2}{2}, \qquad k_I > 0 \tag{9}$$

Where e_I is defined as:

$$e_I = \int_0^t e_{vC} dt = 0 \tag{10}$$

In order to ensure that the time derivative of (9) is negative define:

$$\frac{dV_{L1}}{dt} = k_I e_I \frac{de_I}{dt} + e_{vC}\frac{de_{vC}}{dt} = k_v e_{vC} \tag{11}$$

After some algebraic manipulation of equation (11) and considering (5), the virtual control action is now given by:

$$i_{Lref1} = C\left(k_v e_{vC} + k_I e_I + \frac{dv_{Cref}}{dt}\right) + I_0 \tag{12}$$

b) Sliding Mode Current Controller

Let us consider a function γ defined to characterize the converter operation in Fig. 1:

$$\gamma = \begin{cases} 1 & when\ S\ ON \\ 0 & when\ S\ OFF \end{cases} \tag{13}$$

$$\text{If } \gamma = 1 \qquad v_L = U - V_0 = L\frac{di_L}{dt} > 0 \qquad ,U > V_0 \tag{14}$$

$$\text{If } \gamma = 0 \qquad v_L = -V_0 = L\frac{di_L}{dt} < 0 \qquad ,U > V_0 \tag{15}$$

The current controller objective is to make $i_L = i_{Lref}$, meaning that the error associated with this objective is $e_{iL} = i_{Lref} - i_L$. For control design a time-varying linear surface s is defined as follows:

$$s(i_L) = i_{Lref} - i_L = e_{iL} \tag{16}$$

The Lyapunov's direct method is used as a stable condition to guarantee that the sliding surface is reached after a finite period of time. By defining the Lyapunov function:

$$V_{L2} = \frac{1}{2}s^2 = \frac{e_{i_L}^2}{2} \tag{17}$$

The stability condition is satisfied (i.e. $e_{iL} = 0$), if $\dot{V}_{L2} < 0$. However, in order to achieve a zero error, an infinite switching frequency would be required. So, the error must be bounded by $-\Delta/2 < e_{iL} < +\Delta/2$ and the control action to do so is:

$$\text{If } e_{iL} > +\frac{\Delta}{2} \Rightarrow i_{Lref} > i_L \text{ then, } i_L \uparrow \Rightarrow \frac{di_L}{dt} > \frac{di_{Lref}}{dt} \tag{18}$$

$$\text{If } e_{iL} < -\frac{\Delta}{2} \Rightarrow i_{Lref} < i_L \text{ then, } i_L \downarrow \Rightarrow \frac{di_L}{dt} < \frac{di_{Lref}}{dt} \tag{19}$$

From equation (14) and (15), it is clear in order to guarantee that $di_L/dt > di_{Lref}/dt$, then the semiconductor S must be ON. On the other hand, if $di_L/dt < di_{Lref}/dt$ then the semiconductor S must be OFF.

$$\gamma = \begin{cases} 1 & if \quad e_{iL} > +\Delta/2 \\ 0 & if \quad e_{iL} < -\Delta/2 \end{cases} \tag{20}$$

The signal to drive the semiconductor S is obtained using a hysteresis comparator. This controller is able to provide a fast-dynamic response, is stable and robust to load variations or any type of dynamic perturbations.

2) Recursive Backstepping Control

The first step to design the Recursive Backstepping Controller (RBC) is to derive a virtual control input i_{Lv} to minimize the tracking error of the output voltage $e_{vC} = v_{Cref} - v_C$. The result is the same as the one presented in section 1)a).

$$i_{Lv} = Ck_v e_{v_C} + C\frac{dv_{Cref}}{dt} + I_0 \tag{21}$$

In the second step, to obtain the input control u input that enforces the i_L virtual control input ($i_L = i_{Lv}$), recursively apply the above method by defining the error of the virtual control input:

$$e_{iL} = i_{Lv} - i_L \tag{22}$$

Applying the 2nd method of Lyapunov stability, by proposing a candidate Lyapunov function positive definite:

$$V_i = \frac{e_{vC}^2}{2} + \frac{e_{iL}^2}{2} \tag{23}$$

To make sure that the time derivative of (23) is negative:

$$\dot{V}_i = e_{vC}\left(\frac{dv_{Cref}}{dt} - \frac{i_{Lv} + e_{iL} - I_o}{C}\right) + e_{iL}\left[\frac{di_{Lv}}{dt} - \frac{u - v_C}{L}\right] = -k_v e_{vC}^2 - k_i e_{iL}^2 \tag{24}$$

After some manipulations the control input average value u can be obtained. The duty-cycle average value $\bar{\delta}$, which is the control signal that is going to be applied to a linear modulator that will generate the driving signal for the semiconductor S (Fig. 1), can be obtained from $u = \bar{\delta}U$.

$$\bar{\delta} = \frac{L}{U}\left(e_{vC}\left(\frac{1}{C} - Ck_v^2\right) + e_{iL}\left(k_v + k_i\right) + \frac{dI_o}{dt} + C\frac{d^2 v_{Cref}}{dt^2}\right) + \frac{v_C}{U} \tag{25}$$

IV. RESULTS

A. Simulation Results

In order to evaluate the performance of both controllers, a model of the whole system presented in Chapter II was created in MATLAB/Simulink. The value chosen for the DC grid

voltage was 380V. Table 1 shows the simulation parameters for the main DC/DC converter.

Table 1 - Simulation Parameters of the Main Converter

Input Voltage [V]	Output Voltage [V]	Rated Power [W]	L [mH]	r_l [Ω]	C [µF]	r_c [Ω]	f [kHz]
540	380	3500	6.3	0.4	5.5	1	20

To access if the main DC/DC converter is able to supply the DC grid under a large load variation, three Buck Converters operating at constant power are connected to the grid. The following scenario was simulated:

- At t=0s Converter 1 is connected to the DC grid
- At t=0.05s Converter 2 is connected to the DC grid
- At t=0.05s Converter 3 is connected to the DC grid

Converter 1, 2 and 3 have an efficiency of 95% and their switching frequencies are 20kHz, 30kHz and 40kHz, respectively. All the loads have an input filter (Fig. 2) and a linear voltage and current PI controller. It is out of the scope of this thesis to evaluate the performance of the load converter control system thus their controllers will remain the same throughout the simulations. The parameters for each load are displayed in Table 2.

Table 2 - Simulation Parameters of the Load Converters

DC/DC Converter 1		DC/DC Converter 2		DC/DC Converter 3	
P_{01}	300 W	P_{02}	1300 W	P_{03}	1500 W
V_{01}	300 V	V_{02}	250 V	V_{03}	200 V
C_1	0.17 µF	C_2	0.7 µF	C_3	1.1 µF
L_1	33 mH	L_2	6 mH	L_3	3.3 mH
C_{f1}	0.65 µF	C_{f2}	2.3 µF	C_{f3}	2.5 µF
L_{f1}	7 mH	L_{f2}	1.1 mH	L_{f3}	0.7 mH
r_{cf1}	0.022 Ω	r_{cf2}	0.19 Ω	r_{cf3}	0.22 Ω
r_{lf1}	0.019 Ω	r_{lf2}	0.006 Ω	r_{lf3}	0.005 Ω
r_{p1}	65 Ω	r_{p2}	12 Ω	r_{p3}	10 Ω

Converter 2 and 3 are considered to be high-power converters thus they are connected to the grid through a soft-starter.

1) Backstepping Sliding Mode Control

The results from using the BSMC design discussed in section III.1) are presented here. According to Lyapunov's second method, the only requirement to choose the value for k_v from equation (8) is $k_v > 0$. By looking at expression (7), it can be seen that the solution to that differential equation is given by:

$$e_{v_C} = ce^{-k_v t} \tag{26}$$

This means that the higher the value k_v, the lower the time constant is, resulting in a system that achieves its steady state much faster. However, in terms of control systems, the outer loop (i.e. Voltage controller) must be slower than the inner loop (i.e. Current controller) in order to decouple both dynamics [16] [17]. Since the main convert switching frequency is around 20kHz, the time constant τ must be bigger than 0.05ms (1/20kHz). Therefore, the value chosen for k_v was 10000, which corresponds to τ=0.1ms

From Fig. 3, it can be seen that the output voltage reaches its expected value (380V) after the connection of the high-power converters at t= 0.05s. This controller has a very fast transient response and presents an output voltage ripple of 2V.

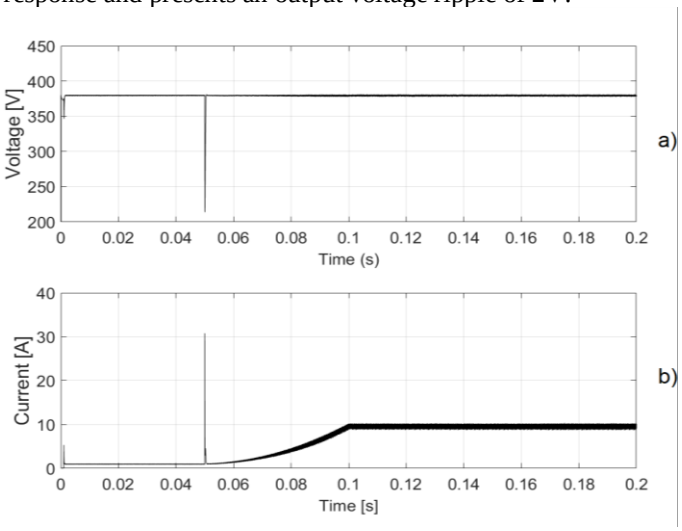

Fig. 3 - Voltage and current waveform in the DC Grid using the BSMC
a) DC grid voltage; b) DC grid current

The system presents no steady state error. However, errors can be observed if there is an offset or another error in one of the measurements. The next picture shows the same experiment but with an error in the output current measurement (I_0) of 20%. The DC grid voltage is shown and it can be seen that there is a steady state error of 40V and the system is unable to reach the desired output voltage.

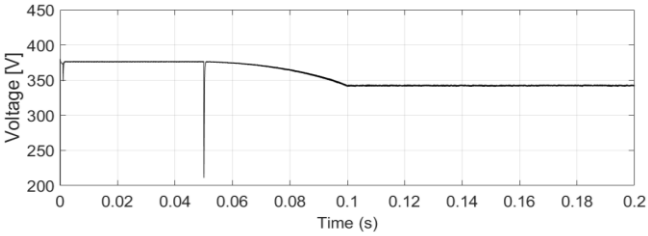

Fig. 4 – Voltage waveforms in the DC Grid using the BSMC with a measurement error

One way to solve this problem is to include an integral action in the controller. The result of using the voltage controller presented in equation (12) is shown in Fig. 5.

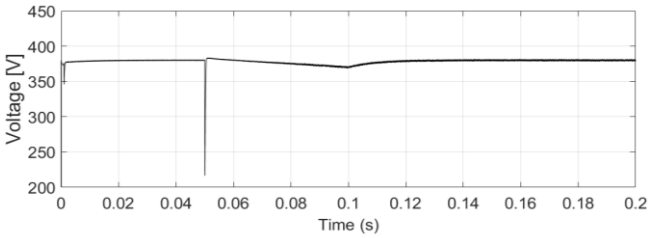

Fig. 5 - Voltage waveform in the DC Grid using the BSMC with a measurement error

2) Recursive Backstepping Control

In order to compare both methods under the same conditions, the gain chosen for k_v, from equation (21) and (25), was also 10000. It's a common practice to select the inner loop gains higher than the output loop gains to achieve good tracking performance [16] [17]. (i.e. $k_i > k_v$), thus the value chosen for k_i was 100000.

A constant frequency modulator was designed for this controller, that guarantees that in a PWM cycle, the converter does not switch more than once. Fig. 6 represents the same test performed in the previous section but using controllers based on backstepping control theory.

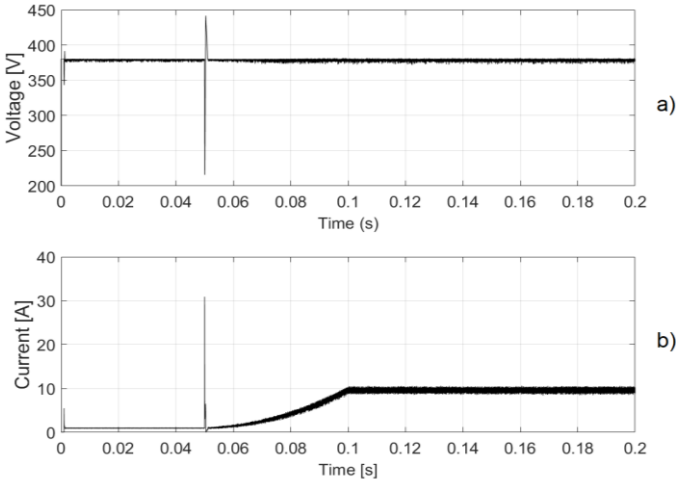

Fig. 6 - Voltage and current waveform in the DC Grid using the RBC with a constant frequency modulator: a) DC grid voltage; b) DC grid current

Fig. 6 shows that the DC grid voltage reaches its equilibrium point (380V) quite fast after a disturbance in the grid. After the connection of converter 2 and 3, the system has 20% overshoot but the control system is able to return to the steady state with a settling time of 1ms.

The results of having an error of 20% in the measurement of the output current are expressed in Fig. 7. It's clear that this controller eliminates the steady-state error as opposed to the controller BSMC described in the previous section.

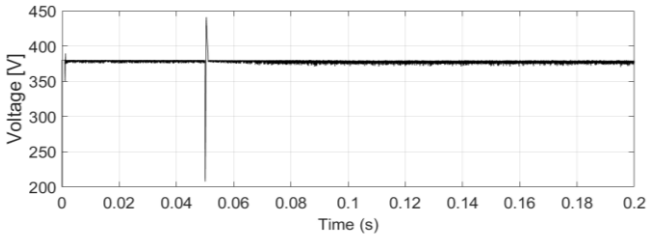

Fig. 7 - Voltage waveform in the DC Grid using the RBC with a measurement error

3) Short-circuit in the grid

In this thesis, the circuit breaker (CB) has been modelled as an ideal switch that will open the circuit if the input current of one of the loads has surpassed its correspondent maximum threshold, during a short time interval.

The next figure shows the voltage and current in the DC-grid when a pole-to-ground fault is applied to the second load converter 2 at t=0.1s.

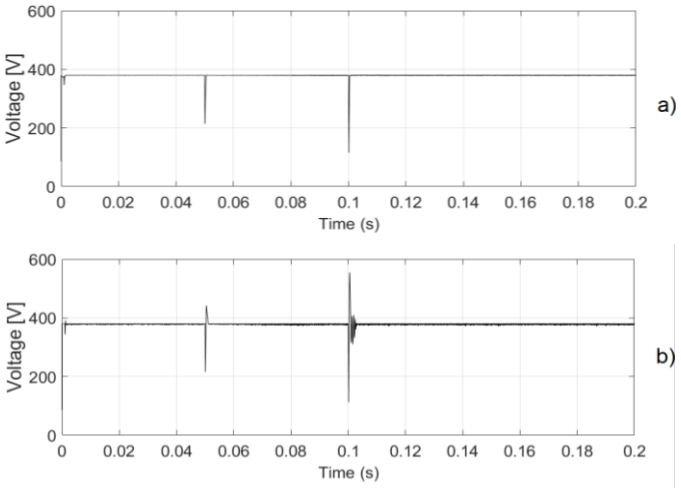

Fig. 8 - Pole-to-ground fault in the converter 2 a) using the BSMC; b) using the RBC

After a short circuit at the input of DC-DC converter 2 a high current spike is detected, the corresponding CB clears the fault by disconnecting the respective load. As seen in both figures above, the main control system is still able to maintain the desired voltage after an abrupt load variation. However, the results also show that the second load induces a large overshoot (≈50%).

The main circuit breaker is supposed to interrupt the current flow when a fault or short circuit occurs in the DC grid. A robust control system should restore the voltage back to its nominal value after the fault on the DC-bus disappears. To restore the DC grid back a recloser is used. A recloser is a special type of CB that has the ability to restore the power automatically in temporary fault situations. A recloser has been simulated in which the number of reclose attempts is limited to a maximum of three in equally spaced time intervals of 0.05s.

Fig. 9 shows a short-circuit on a charged power line at t=0.1s and lasts 0.06s. It can be seen that at t=0.15s the main CB tries to reclose but fails since the short circuit is not extinguished. However, at t=0.2s, the short-circuit has disappeared and all the converters are supplied.

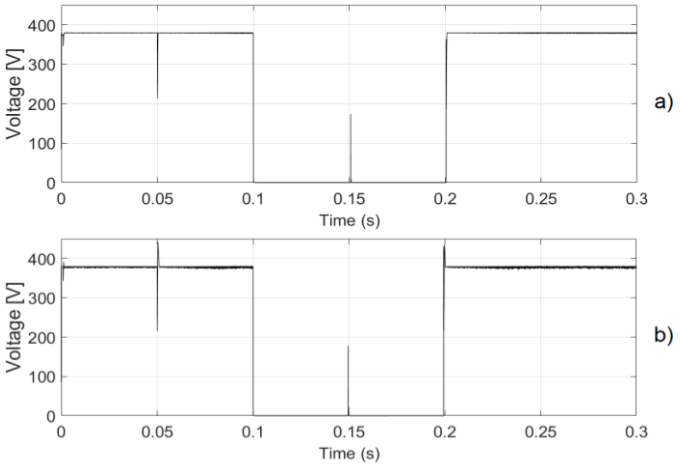

Fig. 9 - Pole-to-ground fault in the Grid a) using the BSMC; b.) using the RBC

B. *Experimental Results*

On a much smaller scale, due to lab restritions and available materials, the results obtained with the Backstepping Sliding Mode Controller on Simulink were reproduced in the Electrical Energy laboratory of Instituto Superior Técnico.

The DC-link voltage was chosen to be 19V, and the control scheme was implemented in a Microchip dsPIC33EP512MU810. The microprocessor receives as input the measurements of the inductor current, DC grid's and DC grid's voltage, and has the task of producing the driving signal for the transistor located in the main DC-DC Converter. The constant power load used in this experiment were HP laptops with a power consumption of 23W. Additionally a 50 ohms resistive load was connected to the DC grid.

Fig. 10 depicts the voltage in the DC grid with a resistor as a load (Fig. 10 a)) and with a resistor and one laptop as a load (Fig. 10 b)). It is clear that after connection of the laptop to the grid the current increases but the DC voltage remains the same.

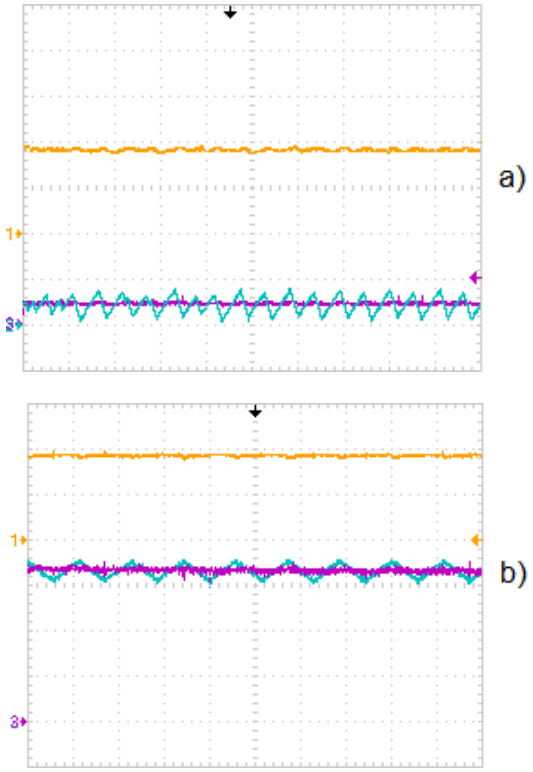

Fig. 10 - DC grid voltage and current waveforms, and inductor's current in the main DC/DC converter: a) Using a resistive load; CH1 (orange): DC grid voltage waveform (10V/div); CH2 (blue): Inductor's current waveform (1A/div); CH3 (purple): DC grid's current waveform (1A/div). *t* (2.5 ms/div) b) Using a resistive load and a laptop computer; CH1 (orange): DC grid voltage waveform (10V/div); CH2 (blue): Inductor's current waveform (0.5A/div); CH3 (purple): DC grid's current waveform (0.5A/div). *t* (250 µs/div)

In Fig. 11 the input voltage U in the main converter (Fig. 1) is increased from 40V to 60V resulting in a smaller duty cycle. Despite the input voltage increase, Fig. 11 shows that the voltage in the DC grid still remains at around 19V.

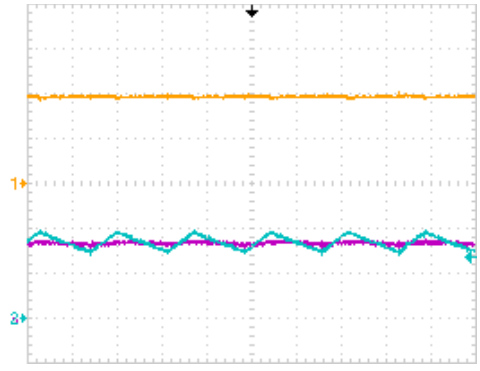

Fig. 11 - Results obtained for the DC grid voltage and current, and inductor's current in the main DC/DC converter; CH1 (orange): DC grid voltage waveform (10V/div); CH2 (blue): Inductor's current waveform (1A/div); CH3 (purple): Grid's current waveform (1A/div) *t*(250 µs/div)

Fig. 12 represents the transient response of the voltage and current in the DC grid. Fig. 12.a) shows the transient when the laptop is connected to the DC grid, and Fig. 12 b) shows the transient when the laptop is disconnected from the DC grid.

The DC grid voltage waveform is zoomed on purpose to show that after the connection/disconnection of the laptop the controller is still able to track the desired value.

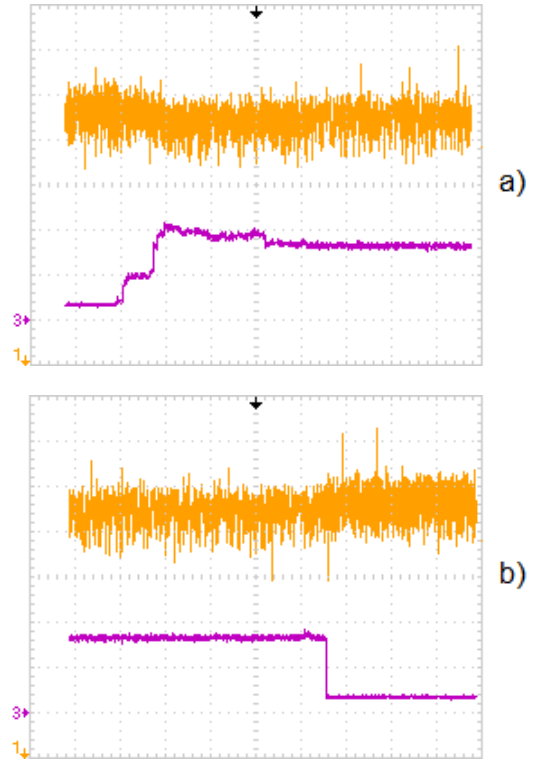

Fig. 12 - Transient response of DC grid voltage and current: a) Transient when the laptop is connected to the DC grid; b) Transient when the laptop is disconnected from the DC grid. CH1 (orange): DC grid voltage (500mV/div), CH3 (purple): DC grid current (1A/div) *t* (1s/div)

The next figure presents the transient response of the grid voltage when two laptops are connected to the DC-link. The second load connected is another HP laptop with a power consumption of 23W.

Fig. 13 - Transient response of DC grid voltage and current when the two laptops are connected to the DC grid CH1 (Orange): DC grid voltage (5V/div) CH2 (Blue): Inductor's current waveform (0.5A/div) t(50ms/div)

There is no voltage sag shown in the figures above mainly because the value of the capacitator is around 20 times bigger than necessary. In Appendix B all the values of the components used in the laboratory experiments are presented.

Non-linear controllers showed favourable results when compared with the results obtained with the well-known linear current and voltage controllers [5] [18].

V. Conclusions

The objective of this paper was to design non-linear controllers for a DC-DC converter that supplies power to a DC microgrid without needing to increase the capacitance of the DC line stabilizing capacitor. Two different non-linear control systems were designed in order to counteract the nonlinearities induced by CPL. The controller's performance was evaluated based on the stability of the DC grid voltage and their transient and dynamic response when a disturbance occurs.

Both the Backstepping Sliding Mode Controller and Recursive Backstepping Controller guaranteed the stability of the DC distribution grid. Through comparative computer simulations, the best performance was obtained with BSMC. Experimental studies conducted on the laboratory of Instituto Superior Técnico validate the proposed BSMC controller.

VI. Acknowledgments

This work was supported by national funds through Fundação para a Ciência e Tecnologia (FCT) with reference UID/CEC/50021/2013

VII. References

[1] D. J. Becker and B. J. Sonnenberg, "400 Vdc Power Distribution: Overcoming the Challanges," in *IEEE 32nd International Telecommunocations Energy Conference*, Orlando, Florida, USA, 2010.

[2] G. Iwanski, P. Staniak and W. Koczara, "Power management in a DC microgrid supported by energy storage," in *2011 IEEE International Symposium on Industrial Electronics*, Gdansk, Poland, 2011.

[3] K. Garbesi, V. Vossos and H. Shen, "Catalog of DC Appliances and Power Systems," Berkeley, California, USA, Oct. 2001.

[4] B. Glasgo, I. L. Azevedo and C. Hendrickson, "How much electricity can we save by using direct current circuits in homes? Understanding the potential for electricity savings and assessing feasibility of a transition towards DC powered buildings," 66-75, 180, Applied Energy.

[5] G. M. Paraíso, J. F. Silva and S. F. Pinto, "Control strategies for low voltage DC residencial grids with constant power loads," in *2018 International Young Engineers Forum (YEF-ECE)*, Lisbon, Portugal, 2018.

[6] L. Herrera, W. Zhang and J. Wang, "Stability Analysis and Controller Design of DC Microgrids With Constant Power Loads," *IEEE Transactions on Smart Grid*, vol. 8, no. 2, pp. 881-888, 2017.

[7] J. Liu, W. Zhang and G. Rizzoni, "Robust Stability Analysis of DC Microgrids With Constant Power Loads,"

IEEE Transactions on Power Systems, vol. 33, no. 1, pp. 851-860, Jan. 2918.

[8] M. Al-Nussairi, R. Bayindir, P. Sanjeevikumar and P. Siano, "Constant Power Loads (CPL) With Microgrids: Problem Definition, Stability Analysis and Compensation Techniques," *Energies,* vol. 10, no. 10, Oct. 2017.

[9] D. Shuai, Y. Xie and X. Wang, "Optimal control of Buck converter by state feedback linearization," in *2008 7th World Congress on Intelligent Control and Automation*, Chongqing, China, Aug. 2008.

[10] L. Setyawan, W. Peng and X. Jianfang, "Implementation of sliding mode control in DC microgrids," in *2014 9th IEEE Conference on Industrial Electronics and Applications*, Hangzhou, China, June 2014.

[11] J. F. Silva, ""Input filter design for power converters" Texto Complementar da disciplina SAA," 2012. [Online]. Available: https://fenix.tecnico.ulisboa.pt/downloadFile/3779578920509/input%20LC%20filters__.pdf.

[12] M. U. Iftikhar, D. Sadarnac and C. Karimi, "Input Filter Damping Design for Control Loop Stability of DC-DC Converters," in *2007 IEEE International Symposium on Industrial Electronics*, Vigo, Spain, 2007.

[13] H. K. Khalil, Nonlinear Systems, New Jersey, USA: Prentice Hall.

[14] S. Zhang and W. Qian, "Dynamic backstepping control for pure-feedback nonlinear systems," *CoRR abs/1706.08641,* 2017.

[15] A. D. Martin, J.M.Cano, F. A. Silva and J. R. Vazquez, "Backstepping Control of Smart-grid Connected Distributed Photovoltaic Power Suplies for Telecom Equipment," *IEEE Transactions on Energy Conversion,* no. 99, 2015.

[16] E. V. Oort, L. Sonneveldt, Q. Chu and J. Mulder, "Full Envelope Modular Adaptive Control of a Fighter," in *AIAA Guidance, Navigation, and Control Conference*, Toronto, Canada, Aug. 2010.

[17] G. F. Trigo, "Robust and Adaptive Nonlinear Attitude Control of a Spacecraft," Instituto Superior Técnico, Universidade de Lisboa, Mcs Thesis, Lisboa, Portugal, Oct. 2011.

[18] G. M. Paraiso, "Design of Control Strategies for Low Voltage DC Residential Grids," Lisbon, Portugal, 2018.

[19] E. V. Oort, L. Sonneveldt, Q. Chu and J. Mulder, "Full Envelope Modular Adaptive Control of a Fighter," in *AIAA Guidance, Navigation, and Control Conference*, Toronto, Canada, Aug. 2010.